Condensed Matter Physics, 2012, Vol. 15, No 3, 33705: 1–20
DOI: 10.5488/CMP.15.33705
http://www.icmp.lviv.ua/journal

CONDENSED MATTER PHYSICS

Longitudinal relaxation of mechanically clamped KH_2PO_4 type crystals

R.R. Levitskii[1], I.R. Zachek[2], A.S. Vdovych[1]

[1] Institute for Condensed Matter Physics of the National Academy of Sciences of Ukraine, 1 Svientsitskii Str., 79011 Lviv, Ukraine

[2] Lviv Polytechnic National University, 12 Bandera Str., 79013 Lviv, Ukraine

Received January 27, 2012, in final form July 4, 2012

Within the framework of a modified proton ordering model of the KH_2PO_4 family ferroelectric crystals, taking into account a linear over the strain ε_6 contribution into the proton system energy, we obtain an expression for longitudinal dynamic dielectric permittivity of a mechanically clamped crystal using the four-particle cluster approximation and the dynamic Glauber approach. At a proper choice of the model parameters, we obtain a good quantitative description of available experimental data for these crystals.

Key words: *ferroelectric, cluster approximation, dielectric permittivity, relaxation times*

PACS: *77.84.-s, 77.22.-d, 77.80.-e, 77.22.Ch*

1. Introduction

In the late 1960-ies, most theoretical and experimental studies of ferroelectrics concentrated on various dynamic phenomena. The dispersion of dielectric permittivity of ferroelectrics was explored at low frequencies, which provided an important information on the mechanisms of phase transitions and revealed the peculiarities of the low-frequency dynamics of a system. Ferroelectric dispersion is closely related to the presence of a low-frequency excitation, i.e., a soft mode which can be either resonant or relaxational. Ferroelectric compounds of the KH_2PO_4 family occupy an intermediate position. The region of fundamental dispersion in these crystals is located in the submillimeter range $\nu \approx 50$ GHz. At deuteration, the ferroelectric dispersion in these crystals is shifted to the millimeter and microwave ranges.

The major task of dielectric spectra studies of ferroelectric crystals is to explore the peculiarities of the soft mode behavior, especially in the phase transition region [1]. As a rule, the soft modes in the KH_2PO_4 family ferroelectrics are strongly damped. To explore their character is a complicated task. One has to explore the dielectric spectra of these crystals in a wide frequency range that includes several regions requiring specific and unique experimental methods of measurements. There is hardly any experimental group fully equipped for such studies. This fact, along with the principal difficulties in experimental measurements of dielectric spectra, and the dependence of $\hat{\varepsilon}^*(\omega, T)$ on sample quality and surface treatment, causes the situation when the experimental data for dielectric spectra of the KH_2PO_4 family ferroelectrics turn out to be disembodied and quite conflicting. This should be kept in mind while analysing the experimental data and the theoretical results for dynamic characteristics of ferroelectrics including those of the KH_2PO_4 family.

In the late 1970-ies, the obtained experimental results for the dynamic characteristics in the KH_2PO_4 family compounds were interpreted mostly within phenomenological models (see [1–3]). Phenomenological theories do not make it possible to reveal the microscopic nature of the dispersion of dielectric permittivity or to appropriately describe the effect of various factors on the character of its temperature and frequency dependencies. The attempts to solve this problem using the Green's function method or Bloch kinetic equations method failed [4, 5].

A vast majority of studies on the theory of relaxation phenomena in the KH_2PO_4 family ferroelectrics are based on the stochastic Glauber model [6]. For the first time, the relaxation dynamics of the KD_2PO_4 type ferroelectrics was studied using this method in [2], where, within the four-particle cluster approximation (FPCA), there was initiated a study of the main regularities of longitudinal relaxation in the case of a paraelectric phase. However, long-range interactions were not taken into account therein, and the corresponding experimental data for the KD_2PO_4 type ferroelectrics were not discussed. Later on [7–9], a more consistent model of deuterated KD_2PO_4 type ferroelectrics and $ND_4D_2PO_4$ type antiferroelectrics was explored. Within the framework of this model, using the FPCA for short-range interactions and the mean field approximation for long-range interactions, longitudinal dynamic characteristics of these crystals were calculated. It was shown [10–12] that the theory proposed in [7–9] provides a satisfactory description of thermodynamic and longitudinal dynamic characteristics of the KH_2PO_4 type ferroelectrics. In [13–15], the authors attempted to develop a more consistent theory of the KH_2PO_4 family ferroelectrics in the FPCA which takes tunneling (Ω) into account. The results were not good enough to appropriately describe the available experimental data for the dynamic characteristics of these crystals. However, the fact of suppression of the dynamic characteristics of the KH_2PO_4 type ferroelectrics by short-range interactions was established. An effective tunneling parameter $\tilde{\Omega}$ ($\tilde{\Omega} \ll \Omega$) renormalized by the short-range interactions was obtained. It should be noted that the established in [13–15] suppression of dynamic characteristics of the KH_2PO_4 type ferroelectrics by short-range correlations is the most probable reason of the Debye-type dispersion of dielectric permittivity observed in these crystals.

In [16–18], thermodynamic and dynamic characteristics of quasi-one-dimensional hydrogen bonded CsH_2PO_4 ferroelectrics were found using a self-consistent approach to the calculation of thermodynamic and dynamic characteristics of pseudospin systems with essential short-range and long-range interactions, based on the calculation of the free energy functional with short-range interactions taken into account in the reference approach. It was established that an essential suppression of the soft vibration mode by short-range correlations takes place in a wide temperature range. This fact, just like in the case of KH_2PO_4, is directly related to the Debye type of longitudinal dielectric permittivity dispersion observed in CsH_2PO_4. It should be mentioned that similar studies of thermodynamic and dynamic characteristics of KH_2PO_4 can be carried out using the technique developed in [19]. Such studies would make it possible to explore the effect of suppression of the soft mode in the KH_2PO_4 type ferroelectrics more consistently than in [13] and thereby to explain the Debye character of the dielectric permittivity dispersion in these crystals.

It should be noted that the ferroelectric compounds of the KH_2PO_4 family are piezoelectric. Piezoelectric coupling is observed in external electric fields and mechanical stresses of certain symmetries. Ferroelectric phase transition in the KH_2PO_4 type crystals is accompanied by the appearance of spontaneous strains, which changes their tetragonal symmetry. So far, the calculations of dielectric characteristics of these crystals within the proton ordering model [1, 2, 7–12] were restricted to a static limit and high-frequency relaxation. The attempts to explore the piezoelectric resonance phenomenon within a model that does not take into account the piezoelectric coupling were vain. The conventional proton ordering model does not permit one to describe the effects associated with the differences of the free and clamped crystal regimes in the static limit or the phenomenon of crystal clamping by a high-frequency field. This leads, in particular, to some quantitative deviations from experiment for the temperature behavior of polarization relaxation time and dynamic dielectric permittivity of the KH_2PO_4 type ferroelectrics in the phase transition region.

The studies of the piezoelectric coupling effect on the phase transition and on physical characteristics of the KH_2PO_4 type ferroelectrics were initiated in[20], where the Slater theory [21] was modified by taking into account the splitting of the lowest ferroelectric level due to the strain ε_6.

The most fundamental results for the KH_2PO_4 family ferroelectrics were obtained in [22–30]. For the deformed crystals of the KH_2PO_4 type, the Hamiltonian of the proton ordering model was modified for the first time by including ε_6 into in the shear strain [22, 23], taking into account the deformational mean field and the splitting of the lateral proton configurations. Later on [24, 25], all possible splittings of proton configurational energies by the strain ε_6 were included into the model. In [24], using this model, the phase transition, thermodynamic and longitudinal dielectric, piezoelectric, and elastic characteristics of $K(H_{0.12}D_{0.88})_2PO_4$, as well as the effect of the σ_6 on these quantities were explored. The same characteristics for other $K(H_{1-x}D_x)_2PO_4$ type ferroelectrics were later on calculated in [26].

The thermodynamic and longitudinal dielectric, piezoelectric, and elastic characteristics of the KH_2PO_4 type were also calculated in [25, 27] within a model that takes into account the tunneling and piezoelectric coupling. It should be mentioned, however, that taking into account the tunneling within the cluster approximation yields a non-physical behavior of the calculated quantities at low temperatures [31]. In [28–30], the effect of the electric field E_3 on the phase transition and on the physical characteristics of $K(H_{0.12}D_{0.88})_2PO_4$ and KH_2PO_4 was explored, and a good agreement with experiment was obtained.

In [24–28], where there was used a model with tunneling, the dynamic characteristics of the KH_2PO_4 family ferroelectrics were not considered. In [32], using a modified proton ordering model proposed in [24], the dynamic dielectric permittivity of a free KH_2PO_4 type crystals was calculated taking into account the dynamics of ε_6 strain. The experimentally observed effects of crystal clamping by a high-frequency electric field and piezoelectric resonance in KH_2PO_4 and KD_2PO_4 crystals were theoretically described for the first time. Peculiarities of the ultrasound attenuation coefficients near the phase transition temperature in these crystals were also described. In [33], we presented a detailed review of the obtained results for longitudinal and transverse static dielectric permittivities, for piezoelectric coefficients, and for elastic constants of several ferroelectric crystals of the KH_2PO_4 family. Moreover, the typical behavior of longitudinal and transverse characteristics of mechanically free KH_2PO_4, Rb_2PO_4, KH_2AsO_4 crystals was shown and the results for temperature and frequency dependencies of longitudinal and transverse dielectric permittivities of KH_2PO_4 were presented, along with the corresponding experimental data.

In the present paper, using the model proposed in [24] we calculate the longitudinal dynamic dielectric permittivity of clamped ferroelectrics of the KH_2PO_4 type and explore its behavior in wide temperature and frequency ranges. Using the obtained results, we perform a detailed analysis of the available experimental data for these crystals.

2. Systems of equations for the time-dependent deuteron distribution functions

We shall consider a system of deuterons moving on the O–D. . . O bonds in deuterated KD_2PO_4 type ferroelectrics. A primitive cell of the Bravais lattice of these crystals consists of two neighboring tetrahedra PO_4 along with four hydrogen bonds attached to one of them (the “A” type tetrahedron). The hydrogen bonds attached to the other tetrahedron (“B” type) belong to the four structural elements surrounding this tetrahedron (figure 1).

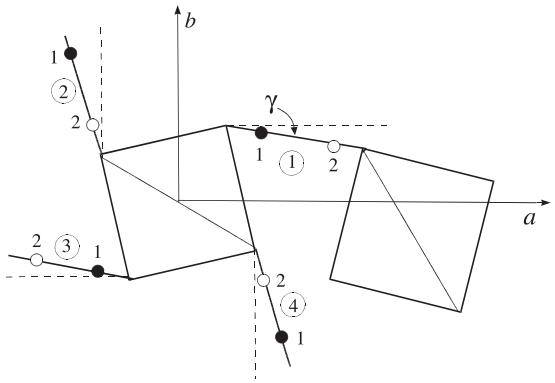

Figure 1. A primitive cell of the KD_2PO_4 type crystal. One of the numerous possible ferroelectric deuteron configurations is shown.

The dynamic characteristics of these compounds will be calculated within the four-particle cluster approximation that proved to be successful in describing their thermodynamic properties [12, 24–27].

The Hamiltonian of the deuteron subsystem, taking into account short-range and long-range interactions in the presence of an external electric field E_3 along the crystallographic c axis and mechanical stress $\sigma_6 = \sigma_{xy}$, which independently contribute to polarization P_3 and strain ε_6, consists of the "seed" and pseudospin parts [24, 26]:

$$\hat{H} = NH^{(0)} + \hat{H}_{\rm s}\,, \tag{2.1}$$

where N is the total number of primitive cells. The "seed" energy of a primitive cell corresponds to the sublattice of heavy ions and does not explicitly depend on the deuteron subsystem configuration. It is expressed in terms of the strain ε_6 and electric field E_3 and includes the elastic, piezoelectric, and dielectric contributions

$$H^{(0)} = v\left(\frac{1}{2}c_{66}^{E0}\varepsilon_6^2 - e_{36}^0 E_3\varepsilon_6 - \frac{1}{2}\chi_{33}^{\varepsilon 0}E_3^2\right), \tag{2.2}$$

where v is the primitive cell volume; c_{66}^{E0}, e_{36}^0, $\chi_{33}^{\varepsilon 0}$ are the "seed" elastic constant, piezoelectric coefficient, and dielectric susceptibility, respectively. They determine the temperature behavior of the corresponding observable quantities at temperatures far from the phase transition $T_{\rm c}$.

The pseudospin part of the Hamiltonian reads

$$\hat{H}_{\rm s} = \frac{1}{2}\sum_{\substack{qf\\ q'f'}} J_{ff'}(qq')\frac{\sigma_{qf}}{2}\frac{\sigma_{q'f'}}{2} + \hat{H}_{\rm sh.s}(6) + \sum_{qf} 2\psi_6\varepsilon_6\frac{\sigma_{qf}}{2} - \sum_{qf}\mu_{f3}E_3\frac{\sigma_{qf}}{2}\,. \tag{2.3}$$

The first term describes effective long-range interactions between deuterons; σ_{qf} is the z-th component of the pseudospin operator that describes the state of a deuteron in the q-th cell on the f-th bond. ($f = 1,2,3,4$). Two eigenvalues of the operator $\sigma_{qf} = \pm 1$ correspond to two possible positions of the deuteron on the bond denoted by "1", "2" in figure 1. In (2.3) $\hat{H}_{\rm sh.s}(6)$ is a linear over the strain ε_6 Hamiltonian of the short-range interactions between deuterons [26]:

$$\begin{aligned}\hat{H}_{\rm sh.s}(6) \;=\; & \sum_q \Bigg[\left(\frac{\delta_{s6}}{8}\varepsilon_6 - \frac{\delta_{16}}{4}\varepsilon_6\right)\left(\sigma_{q1}+\sigma_{q2}+\sigma_{q3}+\sigma_{q4}\right)\\ & -\left(\frac{\delta_{s6}}{8}\varepsilon_6 + \frac{\delta_{16}}{4}\varepsilon_6\right)\left(\sigma_{q1}\sigma_{q2}\sigma_{q3}+\sigma_{q1}\sigma_{q2}\sigma_{q4}+\sigma_{q1}\sigma_{q3}\sigma_{q4}+\sigma_{q2}\sigma_{q3}\sigma_{q4}\right)\\ & +\frac{1}{4}\left(V_{\rm s}+\delta_{a6}\varepsilon_6\right)\left(\sigma_{q1}\sigma_{q2}+\sigma_{q3}\sigma_{q4}\right) + \frac{1}{4}\left(V_{\rm s}-\delta_{a6}\varepsilon_6\right)\left(\sigma_{q2}\sigma_{q3}+\sigma_{q4}\sigma_{q1}\right)\\ & +\frac{1}{4}U_{\rm s}\left(\sigma_{q1}\sigma_{q3}+\sigma_{q2}\sigma_{q4}\right) + \frac{1}{16}\Phi_{\rm s}\sigma_{q1}\sigma_{q2}\sigma_{q3}\sigma_{q4}\Bigg]\,.\end{aligned} \tag{2.4}$$

Here

$$V_{\rm s} = -\frac{1}{2}w_1, \qquad U_{\rm s} = \frac{1}{2}w_1 - \varepsilon, \qquad \Phi_{\rm s} = 4\varepsilon - 8w + 2w_1$$

and

$$\varepsilon = \varepsilon_a - \varepsilon_s, \qquad w = \varepsilon_1 - \varepsilon_s, \qquad w_1 = \varepsilon_0 - \varepsilon_s\,,$$

where $\varepsilon_s, \varepsilon_a, \varepsilon_1, \varepsilon_0$ are the energies of deutron configurations near the PO_4 group.

The third term in (2.3) is a linear over the shear strain ε_6 mean field Hamiltonian induced by the piezoelectric coupling; ψ_6 is the parameter of the deformational mean field.

The last term in (2.3) effectively describes the interactions of deuterons with an external electric field E_3. Here μ_{f3} is the effective dipole moment related to the f-th hydrogen bonds, where

$$\mu_{13} = \mu_{23} = \mu_{33} = \mu_{43} = \mu_3\,,$$

and μ_3 is the dipole moment of up/down deuteron configurations.

Taking into account the peculiarities of the crystalline structure of the MD_2XO_4 the type ferroelectrics, their dynamic characteristics can be calculated within the four-particle cluster approximation that proved to be effective in describing the thermodynamic characteristics of these crystals [12, 24–27].

Long-range interactions are taken into account in the mean field approximation. Within the cluster approach, the thermodynamic potential of MD_2XO_4 ferroelectrics calculated per one primitive cell reads

$$g_{\rm s}(6) = H^{(0)} + 2\nu_{\rm c}\left(\eta^{(1)z}\right)^2 + \frac{1}{2\beta}\sum_{f=1}^{4}\ln Z_{f{\rm s}}^{(1)} - \frac{1}{\beta}\ln Z_{6{\rm s}}^{(4)} - \nu\sigma_6\varepsilon_6\,, \tag{2.5}$$

where $4\nu_{\rm c} = J_{11}(0) + 2J_{12}(0) + J_{13}(0)$, the eigenvalues of Fourier-transform of the long-range interaction matrix $J_{ff'} = \sum\limits_{\mathbf{R}_q - \mathbf{R}_{q'}} J_{ff'}(qq')$;

$$\eta^{(1)z} = \langle\sigma_{q1}\rangle = \langle\sigma_{q2}\rangle = \langle\sigma_{q3}\rangle = \langle\sigma_{q4}\rangle$$

is the parameter of deuteron ordering; $Z_{f{\rm s}}^{(1)} = {\rm Sp}\,{\rm e}^{-\beta\hat{H}_{qf{\rm s}}^{(1)}}$, $Z_{6{\rm s}}^{(4)} = {\rm Sp}\,{\rm e}^{-\beta\hat{H}_{q{\rm s}}^{(4)}}$, $\beta = \frac{1}{k_{\rm B}T}$ are the single-particle and four-particle partition functions. The single-particle $\hat{H}_{qf{\rm s}}^{(1)}$ and four-particle $\hat{H}_{q{\rm s}}^{(4)}$ deuteron Hamiltonians are presented by

$$\hat{H}_{qf{\rm s}}^{(1)} = -\frac{\bar{z}_6}{\beta}\frac{\sigma_{qf}}{2}, \tag{2.6}$$

$$\hat{H}_{q{\rm s}}^{(4)} = -\sum_{f=1}^{4}\frac{z_6}{\beta}\frac{\sigma_{qf}}{2} + \hat{H}_{\rm sh.s}(6), \tag{2.7}$$

where

$$z_6 = \beta\left(-\Delta_{\rm s}^{\rm c} + 2\nu_{\rm c}\eta^{(1)z} - 2\psi_6\varepsilon_6 + \mu_3 E_3\right), \qquad \bar{z}_6 = \beta\left(-2\Delta_{\rm s}^{\rm c} + 2\nu_{\rm c}\eta^{(1)z} - 2\psi_6\varepsilon_6 + \mu_3 E_3\right).$$

The effective field $\Delta_{\rm s}^{\rm c}$ exerted by the neighboring hydrogen bonds from outside the cluster, is determined from the self-consistency condition: the mean values $\langle\sigma_{qf}\rangle$ calculated within the four-particle and one-particle cluster approximations should coincide.

The dynamic characteristics of the MD_2XO_4 crystals will be explored using the proposed dynamic model based on a stochastic Glauber model [6]. Using the method developed in [10–12, 32], the system of equations for the time-dependent deuteron distribution functions is obtained in the form

$$-\alpha\frac{{\rm d}}{{\rm d}t}\left\langle\prod_f\sigma_{qf}\right\rangle = \sum_{f'}\left\{\left\langle\prod_f\sigma_{qf}\left[1 - \sigma_{qf'}\tanh\frac{1}{2}\beta\boldsymbol{\varepsilon}_{qf'}^{z}(t)\right]\right\rangle\right\}, \tag{2.8}$$

where $\boldsymbol{\varepsilon}_{qf'}^{z}(t)$ is the local field acting on the f'-th deuteron in the q-th cell, which can be obtained from the Hamiltonian (2.3). Expanding $\tanh\frac{1}{2}\beta\boldsymbol{\varepsilon}_{qf'}^{z}(t)$ over the pseudospin operators σ_{qf}, occurring in Hamiltonian (2.3), taking into account the fact that $\sigma_{qf} = \pm 1$ and the symmetry of the deuteron distribution functions in the MD_2XO_4 ferroelectrics in the presence of the electric field E_3

$$\begin{aligned}
\eta^{(1)z} &= \langle\sigma_{q1}\rangle = \langle\sigma_{q2}\rangle = \langle\sigma_{q3}\rangle = \langle\sigma_{q4}\rangle,\\
\eta^{(3)z} &= \langle\sigma_{q1}\sigma_{q2}\sigma_{q3}\rangle = \langle\sigma_{q1}\sigma_{q3}\sigma_{q4}\rangle = \langle\sigma_{q1}\sigma_{q2}\sigma_{q4}\rangle = \langle\sigma_{q2}\sigma_{q3}\sigma_{q4}\rangle,\\
\eta_1^{(2)z} &= \langle\sigma_{q2}\sigma_{q3}\rangle = \langle\sigma_{q1}\sigma_{q4}\rangle, \qquad \eta_2^{(2)z} = \langle\sigma_{q1}\sigma_{q2}\rangle = \langle\sigma_{q3}\sigma_{q4}\rangle, \qquad \eta_3^{(2)z} = \langle\sigma_{q1}\sigma_{q3}\rangle = \langle\sigma_{q2}\sigma_{q4}\rangle,
\end{aligned} \tag{2.9}$$

from (2.7), one can obtain a closed system of equations for the time-dependent single-particle, three-particle, and pair distribution functions of deuterons in MD_2XO_4 within the four-particle cluster approximation and for a single-particle distribution function within the single-particle approximation [32]:

$$\alpha\frac{{\rm d}}{{\rm d}t}\begin{pmatrix}\eta^{(1)z}\\ \eta^{(3)z}\\ \eta_1^{(2)z}\\ \eta_2^{(2)z}\\ \eta_3^{(2)z}\end{pmatrix} = \begin{pmatrix}\bar{c}_{11} & \bar{c}_{12} & \bar{c}_{13} & \bar{c}_{14} & \bar{c}_{15}\\ \bar{c}_{21} & \bar{c}_{22} & \bar{c}_{23} & \bar{c}_{24} & \bar{c}_{25}\\ \bar{c}_{31} & \bar{c}_{32} & \bar{c}_{33} & \bar{c}_{34} & \bar{c}_{35}\\ \bar{c}_{41} & \bar{c}_{42} & \bar{c}_{43} & \bar{c}_{44} & \bar{c}_{45}\\ \bar{c}_{51} & \bar{c}_{52} & \bar{c}_{53} & \bar{c}_{54} & \bar{c}_{55}\end{pmatrix}\begin{pmatrix}\eta^{(1)z}\\ \eta^{(3)z}\\ \eta_1^{(2)z}\\ \eta_2^{(2)z}\\ \eta_3^{(2)z}\end{pmatrix} + \begin{pmatrix}\bar{c}_1\\ \bar{c}_2\\ \bar{c}_3\\ \bar{c}_4\\ \bar{c}_5\end{pmatrix}, \tag{2.10}$$

where the following notations are used

$$\begin{aligned}
&\bar{c}_{11}=-(1-P_6^z-Q_{61}^z-Q_{62}^z), && \bar{c}_{12}=R_6^z, && \bar{c}_{13}=M_{61}^z, && \bar{c}_{14}=M_{62}^z, && \bar{c}_{15}=N_6^z, && \bar{c}_1=L_6^z,\\
&\bar{c}_{21}=(2P_6^z+2Q_{61}^z+2Q_{62}^z+3R_6), && \bar{c}_{22}=-(3-P_6^z-Q_{61}^z-Q_{62}^z), && \bar{c}_{23}=(N_6^z+M_{62}^z+L_6^z),\\
&\bar{c}_{24}=(N_6^z+M_{61}^z+L_6^z), && \bar{c}_{25}=(M_{61}^z+M_{62}^z+L_6^z), && \bar{c}_2=(N_6^z+M_{61}^z+M_{62}^z),\\
&\bar{c}_{31}=2(N_6^z+M_{62}^z+L_6^z), && \bar{c}_{32}=2M_{61}^z, && \bar{c}_{33}=-2(1-R_6^z), && \bar{c}_{34}=2P_6^z, && \bar{c}_{35}=2Q_{61}^z, && \bar{c}_3=2Q_{62}^z,\\
&\bar{c}_{41}=2(N_6^z+M_{61}^z+L_6^z), && \bar{c}_{42}=2M_{62}^z, && \bar{c}_{43}=2P_6^z, && \bar{c}_{44}=-2(1-R_6^z), && \bar{c}_{45}=2Q_{62}^z, && \bar{c}_4=2Q_{61}^z,\\
&\bar{c}_{51}=2(M_{61}^z+M_{62}^z+L_6^z), && \bar{c}_{52}=2N_6^z, && \bar{c}_{53}=2Q_{61}^z, && \bar{c}_{54}=2Q_{62}^z, && \bar{c}_{55}=-2(1-R_6^z), && \bar{c}_5=2P_6^z,
\end{aligned} \tag{2.11}$$

$$\alpha\frac{\mathrm{d}}{\mathrm{d}t}\eta^{(1)z}=-\eta^{(1)z}+\tanh\frac{1}{2}\bar{z}_6. \tag{2.12}$$

3. Relaxational dynamics of mechanically clamped MD_2XO_4 crystals

Now, using the obtained systems of equations, let us calculate the dynamic characteristics of the MD_2XO_4 crystals. Let us consider the case of small deviations of the considered system from equilibrium. We can separate the static and dynamic parts in the obtained system of equations. To do so, we present the distribution functions and the effective fields as sums of the equilibrium functions and their fluctuations

$$\begin{aligned}
&\eta^{(1)z}=\eta^{(1)}+\eta_t^{(1)z}, \qquad \eta^{(3)z}=\eta^{(3)}+\eta_t^{(3)z}, \qquad \eta_i^{(2)z}=\eta_i^{(2)}+\eta_{it}^{(2)z} \qquad (i=1,2,3),\\
&z_6=\tilde{z}_6+z_{6t}, \qquad \tilde{z}_6=-\beta\tilde{\Delta}_{\mathrm{s}}^c+2\beta\nu_c\eta^{(1)}-2\beta\psi_6\varepsilon_6, \qquad z_{6t}=-\beta\Delta_{st}^c+2\beta\nu_c\eta_t^{(1)z}+\beta\mu_3E_{3t}.
\end{aligned} \tag{3.1}$$

Owing to a piezoelectric coupling, time-dependent electric fields should induce time-dependent strains. However, in the present paper we shall consider the fields with the frequencies of the order of $10^9\sim10^{12}$ Hz, which is far above the frequency of piezoelectric resonance. When the frequency is that high, the strains are not capable of following the external fields, which means that the crystal is effectively clamped. Therefore, in the expansions (3.1) we assume the strain ε_6 to be time-independent.

We expand the expressions for the coefficients $P_6^z,\ldots,L_6^z$ in series in $z_{6t}/2$ up to the linear terms. Taking into account these expansions and (3.1), we obtain a system of equations that describes the behavior of fluctuational parts of distribution functions [32, 34]:

$$\frac{\mathrm{d}}{\mathrm{d}t}\begin{pmatrix}\eta_t^{(1)z}\\ \eta_t^{(3)z}\\ \eta_{1t}^{(2)z}\\ \eta_{2t}^{(2)z}\\ \eta_{3t}^{(2)z}\end{pmatrix}=\begin{pmatrix}c_{11}&c_{12}&c_{13}&c_{14}&c_{15}\\ c_{21}&c_{22}&c_{23}&c_{24}&c_{25}\\ c_{31}&c_{32}&c_{33}&c_{34}&c_{35}\\ c_{41}&c_{42}&c_{43}&c_{44}&c_{45}\\ c_{51}&c_{52}&c_{53}&c_{54}&c_{55}\end{pmatrix}\begin{pmatrix}\eta_t^{(1)z}\\ \eta_t^{(3)z}\\ \eta_{1t}^{(2)z}\\ \eta_{2t}^{(2)z}\\ \eta_{3t}^{(2)z}\end{pmatrix}-\frac{\mu_3E_{3t}}{2kT}\begin{pmatrix}c_1\\ c_2\\ c_3\\ c_4\\ c_5\end{pmatrix}, \tag{3.2}$$

where the coefficients of the system read

$$\begin{aligned}
&c_{11}=\frac{1}{\alpha}\Big(\bar{c}_{11}^{(0)}+\beta\nu_cY_s^{(1)}-k_s^{(1)}\Psi_s^z\Big), && c_{12}=\frac{1}{\alpha}\Big(\bar{c}_{12}^{(0)}-k_s^{(1)}\bar{c}_{12}^{(0)}\Big), && c_{13}=\frac{1}{\alpha}\Big(\bar{c}_{13}^{(0)}-k_s^{(1)}\bar{c}_{13}^{(0)}\Big),\\
&c_{14}=\frac{1}{\alpha}\Big(\bar{c}_{14}^{(0)}-k_s^{(1)}\bar{c}_{14}^{(0)}\Big), && c_{15}=\frac{1}{\alpha}\Big(\bar{c}_{15}^{(0)}-k_s^{(1)}\bar{c}_{15}^{(0)}\Big), && c_1=\frac{1}{\alpha}k_s^{(1)}r_s,\\
&c_{21}=\frac{1}{\alpha}\Big(\bar{c}_{21}^{(0)}+\beta\nu_cY_s^{(3)}-k_s^{(3)}\Psi_s^z\Big), && c_{22}=\frac{1}{\alpha}\Big(\bar{c}_{22}^{(0)}-k_s^{(3)}\bar{c}_{12}^{(0)}\Big), && c_{23}=\frac{1}{\alpha}\Big(\bar{c}_{23}^{(0)}-k_s^{(3)}\bar{c}_{13}^{(0)}\Big),\\
&c_{24}=\frac{1}{\alpha}\Big(\bar{c}_{24}^{(0)}-k_s^{(3)}\bar{c}_{14}^{(0)}\Big), && c_{25}=\frac{1}{\alpha}\Big(\bar{c}_{25}^{(0)}-k_s^{(3)}\bar{c}_{15}^{(0)}\Big), && c_2=\frac{1}{\alpha}k_s^{(3)}r_s,
\end{aligned}$$

$$c_{31}=\frac{1}{\alpha}\left(\bar{c}_{31}^{(0)}+\beta\nu_c Y_{s1}^{(2)}-k_{s1}^{(2)}\Psi_s^z\right),\qquad c_{32}=\frac{1}{\alpha}\left(\bar{c}_{32}^{(0)}-k_{s1}^{(2)}\bar{c}_{12}^{(0)}\right),\qquad c_{33}=\frac{1}{\alpha}\left(\bar{c}_{33}^{(0)}-k_{s1}^{(2)}\bar{c}_{13}^{(0)}\right),$$
$$c_{34}=\frac{1}{\alpha}\left(\bar{c}_{34}^{(0)}-k_{s1}^{(2)}\bar{c}_{14}^{(0)}\right),\qquad c_{35}=\frac{1}{\alpha}\left(\bar{c}_{35}^{(0)}-k_{s1}^{(2)}\bar{c}_{15}^{(0)}\right),\qquad c_3=\frac{1}{\alpha}k_{s1}^{(2)}r_s,$$
$$c_{41}=\frac{1}{\alpha}\left(\bar{c}_{41}^{(0)}+\beta\nu_c Y_{s2}^{(2)}-k_{s2}^{(2)}\Psi_s^z\right),\qquad c_{42}=\frac{1}{\alpha}\left(\bar{c}_{42}^{(0)}-k_{s2}^{(2)}\bar{c}_{12}^{(0)}\right),\qquad c_{43}=\frac{1}{\alpha}\left(\bar{c}_{43}^{(0)}-k_{s2}^{(2)}\bar{c}_{13}^{(0)}\right),$$
$$c_{44}=\frac{1}{\alpha}\left(\bar{c}_{44}^{(0)}-k_{s2}^{(2)}\bar{c}_{14}^{(0)}\right),\qquad c_{45}=\frac{1}{\alpha}\left(\bar{c}_{45}^{(0)}-k_{s2}^{(2)}\bar{c}_{15}^{(0)}\right),\qquad c_4=\frac{1}{\alpha}k_{s2}^{(2)}r_6,$$
$$c_{51}=\frac{1}{\alpha}\left(\bar{c}_{51}^{(0)}+\beta\nu_c Y_{s3}^{(2)}-k_{s3}^{(2)}\Psi_s^z\right),\qquad c_{52}=\frac{1}{\alpha}\left(\bar{c}_{52}^{(0)}-k_{s3}^{(2)}\bar{c}_{12}^{(0)}\right),\qquad c_{53}=\frac{1}{\alpha}\left(\bar{c}_{53}^{(0)}-k_{s3}^{(2)}\bar{c}_{13}^{(0)}\right),$$
$$c_{54}=\frac{1}{\alpha}\left(\bar{c}_{54}^{(0)}-k_{s3}^{(2)}\bar{c}_{14}^{(0)}\right),\qquad c_{55}=\frac{1}{\alpha}\left(\bar{c}_{55}^{(0)}-k_{s3}^{(2)}\bar{c}_{15}^{(0)}\right),\qquad c_5=\frac{1}{\alpha}k_{s3}^{(2)}r_s.$$

The expressions for the quantities entering the coefficients of the system (3.2), are given in [34]; if the piezoelectric coupling is neglected, they coincide with the corresponding expressions of [12].

The system of equations (3.2) is reduced to a non-uniform differential equation with constant coefficients for a single-particle distribution function

$$\ddddot{\eta}_t^{(1)z}+p_4\dddot{\eta}_t^{(1)z}+p_3\ddot{\eta}_t^{(1)z}+p_2\ddot{\eta}_t^{(1)z}+p_1\dot{\eta}_t^{(1)z}+p_0\eta_t^{(1)z}=\frac{\mu_3 E_{3t}}{2}\beta p, \tag{3.3}$$

where $p=-\left[(\mathrm{i}\omega)^4p^{(4)}+(\mathrm{i}\omega)^3p^{(3)}+(\mathrm{i}\omega)^2p^{(2)}+(\mathrm{i}\omega)p^{(1)}+p^{(0)}\right]$. Expressions for coefficients $p_4,\ldots,p^{(0)}$ are presented in [34].

Finally, time-dependent single-particle distribution function is obtained in the following form

$$\eta_t^{(1)z}=\sum_{i=1}^{5}C_i^z\exp\left(-\frac{t}{\tau_i^z}\right)+\frac{\mu_3E_{3t}}{2}\beta\frac{\sum\limits_{k=0}^{4}(\mathrm{i}\omega)^kp^{(k)}}{(\mathrm{i}\omega)^5+\sum\limits_{k=0}^{4}(\mathrm{i}\omega)^kp_k}. \tag{3.4}$$

Here C_i^z are constant coefficients; τ_i^z are relaxation times represented by

$$\tau_i^z=(-q_i^z)^{-1},$$

where q_i^z are roots of the characteristics equation

$$(q^z)^5+p_4(q^z)^4+p_3(q^z)^3+p_2(q^z)^2+p_1(q^z)+p_0=0. \tag{3.5}$$

The dynamic dielectric susceptibility of a clamped crystal is defined as

$$\chi_{33}^{\varepsilon}(\omega,T)=\lim_{E_{3t}\to0}2\frac{\mu_3}{\nu}\frac{\mathrm{d}\eta_t^{(1)z}}{\mathrm{d}E_{3t}}=\frac{\mu_3^2}{\nu}\beta\frac{\sum\limits_{k=0}^{4}(\mathrm{i}\omega)^kp^{(k)}}{(\mathrm{i}\omega)^5+\sum\limits_{k=0}^{4}(\mathrm{i}\omega)^kp_k}=\frac{\mu_3^2}{\nu}\beta\frac{\prod\limits_{i=1}^{5}\tau_i^z\left[\sum\limits_{k=0}^{4}(\mathrm{i}\omega)^kp^{(k)}\right]}{\prod\limits_{i=1}^{5}(1+\mathrm{i}\omega\tau_i^z)}=\sum_{i=1}^{5}\frac{\chi_{3i}}{1+\mathrm{i}\omega\tau_i^z}. \tag{3.6}$$

The coefficients χ_{3i} are found from the following system of equations

$$\begin{pmatrix}n_{11}&n_{12}&n_{13}&n_{14}&n_{15}\\n_{21}&n_{22}&n_{23}&n_{24}&n_{25}\\n_{31}&n_{32}&n_{33}&n_{34}&n_{35}\\n_{41}&n_{42}&n_{43}&n_{44}&n_{45}\\n_{51}&n_{52}&n_{53}&n_{54}&n_{55}\end{pmatrix}\begin{pmatrix}\chi_{31}\\\chi_{32}\\\chi_{33}\\\chi_{34}\\\chi_{35}\end{pmatrix}=\begin{pmatrix}n_1\\n_2\\n_3\\n_4\\n_5\end{pmatrix}. \tag{3.7}$$

Here, the following notations are used

$$n_{11}=\tau_2^z\tau_3^z\tau_4^z\tau_5^z;\quad n_{12}=\tau_1^z\tau_3^z\tau_4^z\tau_5^z;\quad n_{13}=\tau_1^z\tau_2^z\tau_4^z\tau_5^z;\quad n_{14}=\tau_1^z\tau_2^z\tau_3^z\tau_5^z;\quad n_{15}=\tau_1^z\tau_2^z\tau_3^z\tau_4^z;$$
$$n_{21}=\tau_2^z\tau_3^z\tau_4^z+\tau_2^z\tau_3^z\tau_5^z+\tau_2^z\tau_4^z\tau_5^z+\tau_3^z\tau_4^z\tau_5^z;\quad n_{22}=\tau_1^z\tau_3^z\tau_5^z+\tau_1^z\tau_4^z\tau_5^z+\tau_1^z\tau_3^z\tau_4^z+\tau_3^z\tau_4^z\tau_5^z;$$
$$n_{23}=\tau_1^z\tau_2^z\tau_4^z+\tau_1^z\tau_2^z\tau_5^z+\tau_1^z\tau_4^z\tau_5^z+\tau_2^z\tau_4^z\tau_5^z;\quad n_{24}=\tau_1^z\tau_2^z\tau_3^z+\tau_1^z\tau_2^z\tau_5^z+\tau_1^z\tau_3^z\tau_5^z+\tau_2^z\tau_3^z\tau_5^z;$$
$$n_{25}=\tau_1^z\tau_2^z\tau_3^z+\tau_1^z\tau_2^z\tau_4^z+\tau_1^z\tau_3^z\tau_4^z+\tau_2^z\tau_3^z\tau_4^z;\quad n_{31}=\tau_2^z\tau_3^z+\tau_2^z\tau_4^z+\tau_3^z\tau_4^z+\tau_2^z\tau_5^z+\tau_3^z\tau_5^z+\tau_4^z\tau_5^z;$$
$$n_{32}=\tau_1^z\tau_3^z+\tau_1^z\tau_4^z+\tau_1^z\tau_5^z+\tau_3^z\tau_4^z+\tau_3^z\tau_5^z+\tau_4^z\tau_5^z;\quad n_{33}=\tau_1^z\tau_2^z+\tau_1^z\tau_4^z+\tau_1^z\tau_5^z+\tau_2^z\tau_4^z+\tau_2^z\tau_5^z+\tau_4^z\tau_5^z;$$
$$n_{34}=\tau_1^z\tau_2^z+\tau_1^z\tau_3^z+\tau_1^z\tau_5^z+\tau_2^z\tau_3^z+\tau_2^z\tau_5^z+\tau_3^z\tau_5^z;\quad n_{35}=\tau_1^z\tau_2^z+\tau_1^z\tau_3^z+\tau_1^z\tau_4^z+\tau_2^z\tau_3^z+\tau_2^z\tau_4^z+\tau_3^z\tau_4^z;$$
$$n_{41}=\tau_2^z+\tau_3^z+\tau_4^z+\tau_5^z,\qquad n_{42}=\tau_1^z+\tau_3^z+\tau_4^z+\tau_5^z;\qquad n_{43}=\tau_1^z+\tau_2^z+\tau_4^z+\tau_5^z,$$
$$n_{44}=\tau_1^z+\tau_2^z+\tau_3^z+\tau_5^z,\qquad n_{45}=\tau_1^z+\tau_2^z+\tau_3^z+\tau_4^z;\qquad n_{51}=n_{52}=n_{53}=n_{54}=n_{55}=1;$$

$$n_1=\frac{\mu_3^2}{v}\beta\prod_{i=1}^{5}\tau_i^z p^{(4)},\qquad n_2=\frac{\mu_3^2}{v}\beta\prod_{i=1}^{5}\tau_i^z p^{(3)},\qquad n_3=\frac{\mu_3^2}{v}\beta\prod_{i=1}^{5}\tau_i^z p^{(2)},$$
$$n_4=\frac{\mu_3^2}{v}\beta\prod_{i=1}^{5}\tau_i^z p^{(1)},\qquad n_5=\frac{\mu_3^2}{v}\tau_i^z p^{(0)}. \tag{3.8}$$

The complex longitudinal dielectric permittivity of the deuteron subsystem of a mechanically clamped MD_2XO_4 crystal reads

$$\varepsilon_{33}^{\varepsilon'}(\omega,T)=1+4\pi\chi_{33}^{\varepsilon'}(\omega,T),\qquad \varepsilon_{33}^{\varepsilon''}(\omega,T)=4\pi\chi_{33}^{\varepsilon''}(\omega,T).$$

A numerical analysis shows that the most important contribution to the dispersion of $\varepsilon_{33}^{\varepsilon}(\omega,T)$ is made by the first relaxational mode $[\chi_3(1)\gg\chi_3(i)]$, while the dispersion of the complex dielectric permittivity of a mechanically clamped crystal is close to the Debye one. If the piezoelectric coupling is omitted, $\varepsilon_{33}^{\varepsilon}(\omega,T)$ transforms into the expression corresponding to [12].

4. Comparison of the numerical results with experimental data. Discussion

Let us analyse the results of numerical calculations performed within the framework of the proposed model for longitudinal dynamic dielectric characteristics of the $M(H_{1-x}D_x)_2XO_4$ crystals and compare them with the corresponding experimental data. It should be noted that the theory developed in the previous sections, strictly speaking, is valid for the MD_2XO_4 type crystals only. The experimental data are available for the $M(H_{1-x}D_x)_2XO_4$ crystals with different deuterations x $(0\leqslant x\leqslant 1)$. The experimentally established relaxational character of the dielectric dispersion of $\varepsilon_{33}^{*}(\nu,T)$ [35–38] in these crystals, as has been already mentioned, is associated with suppression of tunneling by short-range interactions. Therefore, we shall neglect the effects of proton tunneling in $M(H_{1-x}D_x)_2XO_4$. We shall assume that the proposed theory for these crystals is also valid if we use the averaged effective values of the model parameters

$$\varepsilon(x)=\varepsilon_{\mathrm{H}}(1-x)+\varepsilon_{\mathrm{D}}x,\qquad w(x)=w_{\mathrm{H}}(1-x)+w_{\mathrm{D}}x.$$

In [26], we calculated the static longitudinal, piezoelectric, elastic, and thermal characteristics of the $M(H_{1-x}D_x)_2XO_4$ and explored their dependencies on the values of the model parameters. It was shown that at a proper choice of these values, a good quantitative agreement between the theoretical results and the corresponding experimental data was obtained. These sets of the model parameters are used herein in calculating the dynamic characteristics of $M(H_{1-x}D_x)_2XO_4$.

The parameter α that sets the time scale of the dynamic processes in $M(H_{1-x}D_x)_2XO_4$, is determined from the condition that theoretical results for frequency dependencies of $\varepsilon_{33}^{*}(\nu,T)$ at different temperatures agree with the experimental data. It is assumed that α_{H} weakly depends on temperature

$$\alpha=(P+R|\Delta T|)\cdot 10^{-14},\qquad \Delta T=T-T_{\mathrm{c}}.$$

Table 1. The obtained optimum values of the model parameters for $K(H_{1-x}D_x)_2PO_4$.

x	T_c (K)	T_0 (K)	$\frac{\varepsilon}{k_B}$ (K)	$\frac{w}{k_B}$ (K)	$\frac{\nu_3(0)}{k_B}$ (K)	$\mu_{3-}, 10^{-18}$ (esu·cm)	$\mu_{3+}, 10^{-18}$ (esu·cm)	χ^0_{33}	P_- (s)	R_- (s/K)	P_+ (s)	R_+ (s/K)
0.00	122.5	122.5	56.00	422.0	17.91	1.46	1.71	0.73	0.35	0.0100	0.43	0.0160
0.21	146.0	145.9	63.78	515.8	23.18	1.54	1.79	0.65	0.85	0.0095	1.22	0.0193
0.29	155.0	154.8	66.74	551.5	25.21	1.57	1.82	0.62	1.05	0.0093	1.51	0.0217
0.64	191.0	190.3	79.71	707.8	32.34	1.70	1.96	0.48	1.76	0.0385	2.44	0.0173
0.79	204.0	203.1	85.27	774.8	34.18	1.76	2.02	0.42	1.92	0.0082	2.65	0.0151
0.84	208.0	207.0	87.12	797.1	34.63	1.77	2.03	0.41	2.02	0.0081	2.83	0.0167
0.91	213.2	212.2	89.71	828.4	35.07	1.80	2.06	0.38	2.16	0.0079	2.88	0.0130
0.93	215.0	213.9	90.45	837.3	35.36	1.81	2.07	0.37	2.20	0.0079	3.04	0.0149
0.99	219.0	217.9	92.67	864.1	35.52	1.83	2.09	0.35	2.72	0.0077	4.21	0.0189
1.00	220.1	219.0	93.05	868.6	35.76	1.84	2.10	0.34	2.84	0.0077	4.54	0.0349

x	$\frac{\psi_6}{k_B}$ (K)	$\frac{\delta_{s6}}{k_B}$ (K)	$\frac{\delta_{a6}}{k_B}$ (K)	$\frac{\delta_{16}}{k_B}$ (K)	$c^0_{66}\cdot 10^{-10}$ (dyn/cm^2)	e^0_{36} (esu/cm^2)
0.00	–150.00	82.00	–500.00	–400.00	7.10	1000.00
0.64	–142.73	58.73	–863.64	–400.00	6.59	1727.27
0.84	–140.45	51.45	–977.27	–400.00	6.43	1954.55
0.93	–139.43	48.18	–1028.41	–400.00	6.36	2056.82
1.00	–138.64	45.64	–1068.18	–400.00	6.30	2136.36

Table 2. The obtained optimum values of the model parameters for RbH_2PO_4 and KH_2AsO_4.

	T_c (K)	T_0 (K)	$\frac{\varepsilon}{k_B}$ (K)	$\frac{w}{k_B}$ (K)	$\frac{\nu_3(0)}{k_B}$ (K)	$\mu_{3-}, 10^{-18}$ (esu·cm)	$\mu_{3+}, 10^{-18}$ (esu·cm)	χ^0_{33}
RbH_2PO_4	147.6	147.6	60.00	440.0	29.13	1.50	2.00	0.40
KH_2AsO_4	97.0	95.8	35.50	385.0	17.43	1.61	1.65	0.70

	$\frac{\psi_6}{k_B}$ (K)	$\frac{\delta_{s6}}{k_B}$ (K)	$\frac{\delta_{a6}}{k_B}$ (K)	$\frac{\delta_{16}}{k_B}$ (K)	$c^0_{66}\cdot 10^{-10}$ (dyn/cm^2)	e^0_{36} (esu/cm^2)
RbH_2PO_4	–130.00	50.00	–500.00	–300.00	5.90	3000.00
KH_2AsO_4	–170.00	130.00	–500.00	–500.00	7.50	3000.00

	P_- (s)	R_- ($\frac{s}{K}$)	P_+ (s)	R_+ ($\frac{s}{K}$)
RbH_2PO_4	0.55	0.0080	0.93	0.0140
KH_2AsO_4	0.47	0.0160	0.61	0.0190

The obtained optimum values of the model parameters are presented in table 1 for $K(H_{1-x}D_x)_2PO_4$ and in table 2 for RbH_2PO_4 and KH_2AsO_4.

Note that μ_{3+}, P_+, R_+ and $\mu_{3-}, P_- R_-$ correspond to the paraelectric and ferroelectric phases, respectively. The temperature dependencies of the real and imaginary parts of the permittivity $\varepsilon'_{33}(\nu, T)$ and $\varepsilon''_{33}(\nu, T)$ at different frequencies for the KH_2PO_4, KD_2PO_4, RbH_2PO_4, and KH_2AsO_4 crystals are shown in figures 2–5. Starting from a certain frequency ν_k, the low-frequency maximum in the temperature curve of $\varepsilon'_{33}(\nu, T)$ is replaced with a sharp minimum at $\Delta T = 0$ K which widens and deepens with an increasing frequency that reaches ε^0_{33} at $\nu \sim 10^{12}$ Hz. In KH_2PO_4 $\nu_k = 33.2$ GHz, in KD_2PO_4 $\nu_k = 1.4$ GHz, in RbH_2PO_4 $\nu_k = 20.5$ GHz, in KH_2AsO_4 $\nu_k = 20.8$ GHz. The maximum of $\varepsilon'_{33}(\nu, T)$ at $\Delta T_n = |T_n - T_c|$ decreases and smears out with an increasing frequency, whereas the magnitude of ΔT_n increases. With increasing fre-

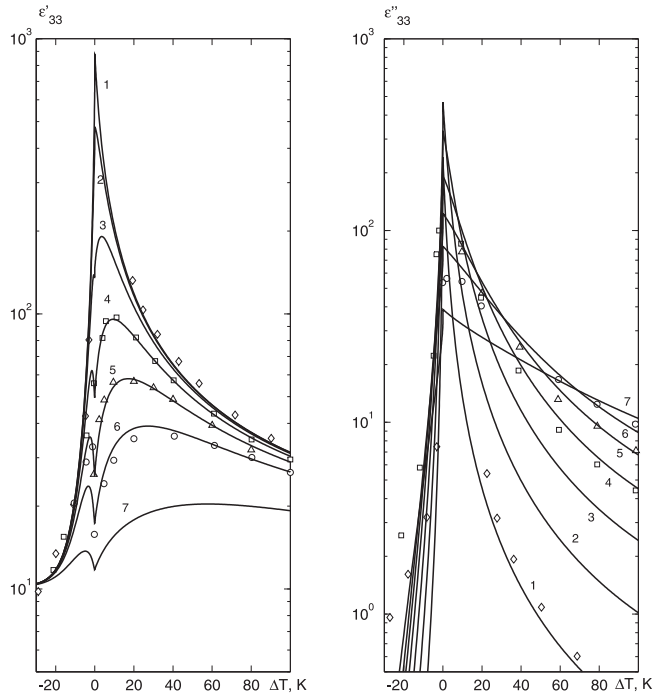

Figure 2. The temperature dependence of ε'_{33} and ε''_{33} in KH_2PO_4 at different frequencies ν (GHz): 9.2 – 1, ◇ [36]; 33.2 – 2; 80 – 3; 154.2 – 4, □ [35]; 249 – 5, △ [35]; 372 – 6, ○ [35]; 800 – 7. Symbols are experimental points; lines are the theoretical values.

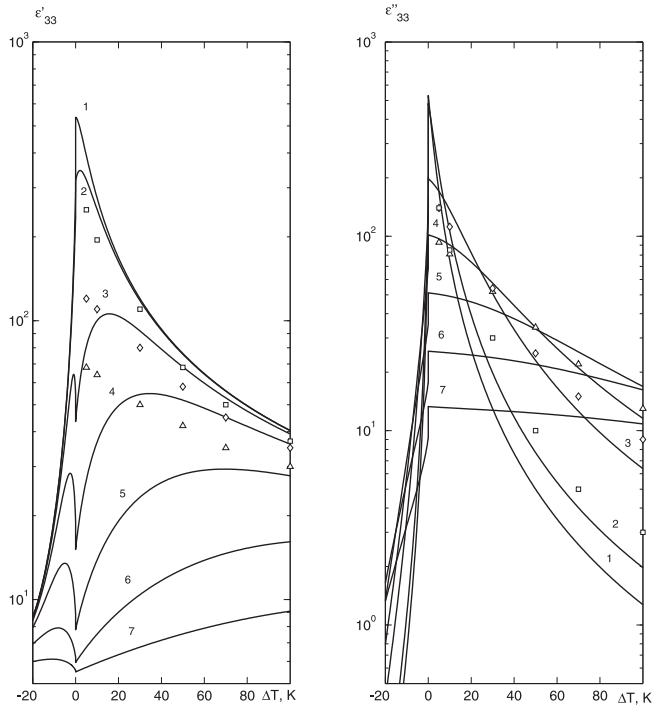

Figure 3. The temperature dependence of ε'_{33} and ε''_{33} in KD_2PO_4 at different frequencies ν (GHz): 1.93 – 1; 3.0 – 2, □ [37]; 10.0 – 3, ◇ [37]; 20.0 – 4, △ [37]; 40.0 – 5; 80.0 – 6; 154.2 – 7. Symbols are experimental points; lines are the theoretical values.

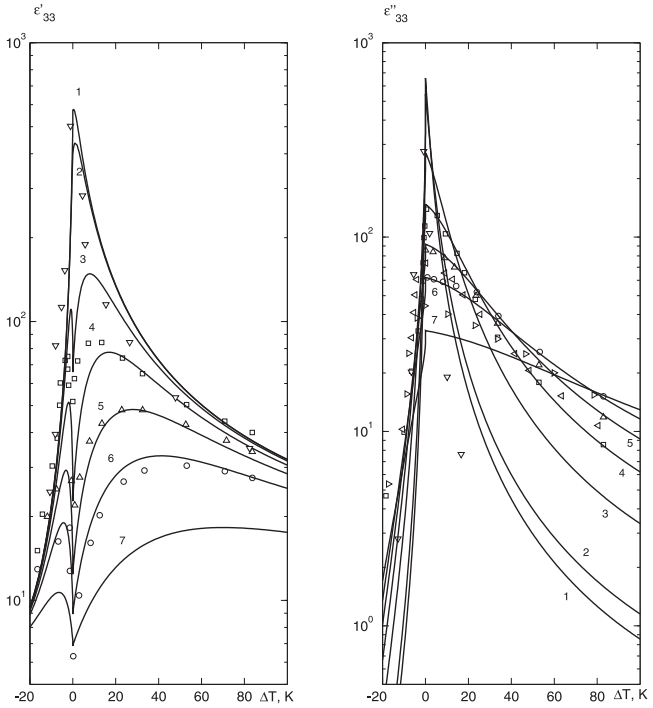

Figure 4. The temperature dependence of ε'_{33} and ε''_{33} in RbH_2PO_4 at different frequencies ν (GHz): 0.25 – 1; 10.0 – 2; 27.0 – 3, ▽ [40]; 154.2 – 4, □ [41]; 250.2 – 5, △ [41]; 372.0 – 6, ○ [41]; 700.0 – 7. Symbols are experimental points; lines are the theoretical values.

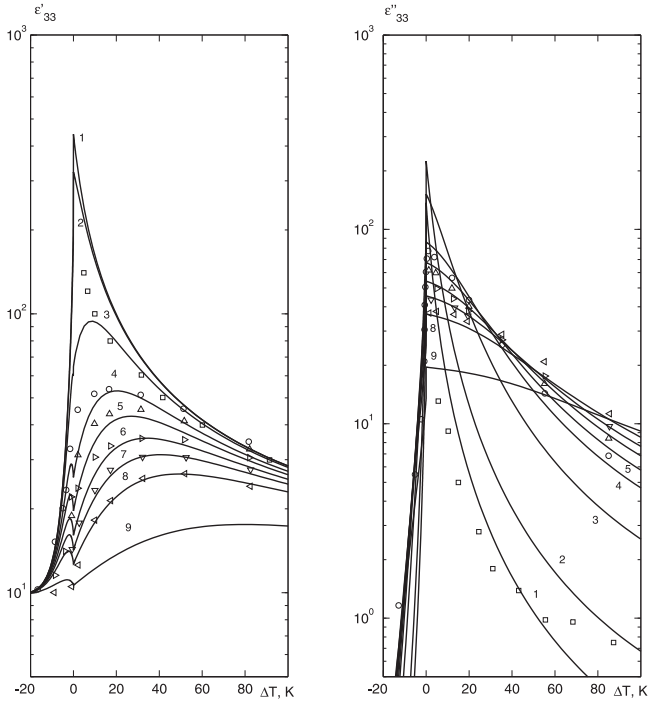

Figure 5. The temperature dependence of ε'_{33} and ε''_{33} in KH_2AsO_4 at different frequencies ν (GHz): 9.2 – 1, □ [36]; 20.8 – 2; 80.0 – 3; 154.2 – 4, ○ [41]; 198.9 – 5, △ [41]; 250.2 – 6, ▷ [41]; 7, ▽ [41]; 372.0 – 8, ◁ [41]; 700.0 – 9. Symbols are experimental points; lines are the theoretical values.

quency the magnitude of $\varepsilon'_{33}(\nu)$ decreases at all $\Delta T = |T - T_c|$. The maximal values of $\varepsilon'_{33}(\nu)$ as well as the values of ΔT_n are much larger in the paraelectric phase than in the ferroelectric phase. The dispersion of a real part of the permittivity $\varepsilon'_{33}(\nu, T)$ in the ferrroelectric phase is observed in a narrow temperature range $\Delta T \sim 20$ K, whereas in the paraelectric phase, ΔT is much larger, being of the order of 200 K.

Let us note that taking into account the piezoelectric coupling, the calculated minimal values of $\varepsilon'_{33}(\nu)$ at $\Delta T = 0$ at different frequencies are larger than those obtained within the model without the piezoelectric coupling.

At a decreasing ΔT in the ferroelectric phase, the value of $\varepsilon''_{33}(\nu)$ increases, has a maximum at $\Delta T = 0$, and decreases with an increasing ΔT in the paraelectric phase. At an increasing frequency, the maximal value of $\varepsilon''_{33}(\nu)$ and the rate of its change with an increasing ΔT diminish.

At ν_k, the values of $\varepsilon'_{33}(\nu, T) = \varepsilon''_{33}(\nu, T)$ are 465 in KH_2PO_4, 520 in KD_2PO_4, 562 in RbH_2PO_4, and 330 in KH_2AsO_4.

The proposed theory provides a good quantitative agreement with the experiment for KH_2PO_4 (figure 2) and a little worse agreement for the data of [37] for KD_2PO_4 (figure 3), especially at $\Delta T < 20$ K for $\varepsilon'_{33}(\nu, T)$. However, it should, be noted that the values of $\varepsilon'_{33}(\nu, T)$ obtained in [37] at frequencies above 1 GHz have maxima at $\Delta T = 0$ K, rather than minima.

The temperature dependence of $\varepsilon^*_{33}(\nu, T)$ in RbH_2PO_4 measured in [41] is appropriately and well described by the present theory, except for the values of $\varepsilon'_{33}(\nu, T)$ at $\nu = 154.2$ GHz and $\Delta T < 20$ K (figure 4). The theory and experimental data of [40] for $\varepsilon^*_{33}(\nu, T)$ at $\nu = 27$ GHz are also in a good agreement. The obtained theoretical results for $\varepsilon^*_{33}(\nu, T)$ at 198 and 366 are only in qualitative agreement with the data of [42], which, in their turn, are in disagreement with the results of other measurements of [41].

The calculated temperature dependencies of $\varepsilon^{\varepsilon'}_{33}(\nu, T)$ and $\varepsilon^{\varepsilon''}_{33}(\nu, T)$ accord well with the ones measured in [41] for KH_2AsO_4 at different frequencies starting from the submillimeter range (figure 5). The data for $\varepsilon^*_{33}(\nu, T)$ obtained in [36] at $\nu = 9.2$ GHz are in a somewhat worse agreement with the theory, especially at $\Delta T < 20$ K.

Figures 6–13 contain the calculated temperature dependencies of the real and imaginary parts of longitudinal dynamic dielectric permittivity $\varepsilon'_{33}(\nu, T)$ and $\varepsilon''_{33}(\nu, T)$ of clamped $K(H_{1-x}D_x)_2PO_4$ crystals at different deuterations x and frequencies along with the corresponding experimental data.

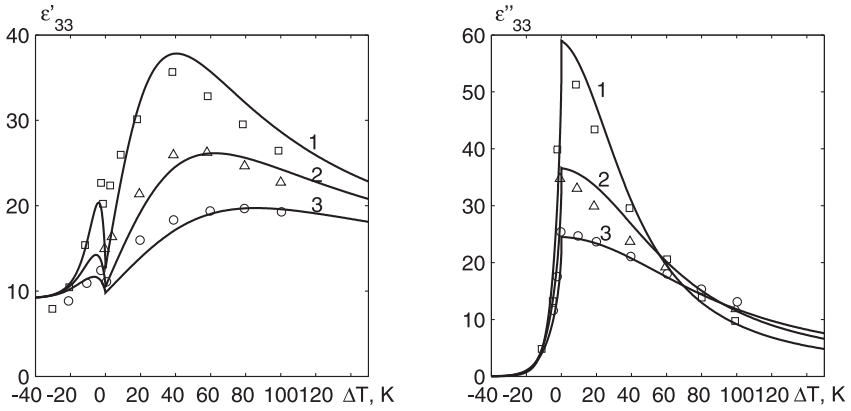

Figure 6. The temperature dependence of ε'_{33} and ε''_{33} in $K(H_{0.79}D_{0.21})_2PO_4$ at different frequencies ν (GHz) [35]: 154.2 – 1, □; 249.0 – 2, △; 372.0 – 3, ○. Symbols are experimental points; lines are the theoretical values.

With an increasing deuteration x in $K(H_{1-x}D_x)_2PO_4$, the magnitude of $\varepsilon'_{33}(\nu, T)$ decreases, whereas ΔT_n increases.

At an isomorphic replacement K → Rb, P→ As, the maximal values of $\varepsilon'_{33}(\nu, T)$ remain almost unchanged, whereas ΔT_n slightly increase.

It should be noted that in the MH_2XO_4, the experimental data of [36, 41, 44, 45] correspond to the region of dielectric permittivity dispersion. At the same time, for KD_2PO_4 in the measurements of [35], the submillimeter frequencies correspond to a high-frequency “tail” of the dispersion, whereas in the

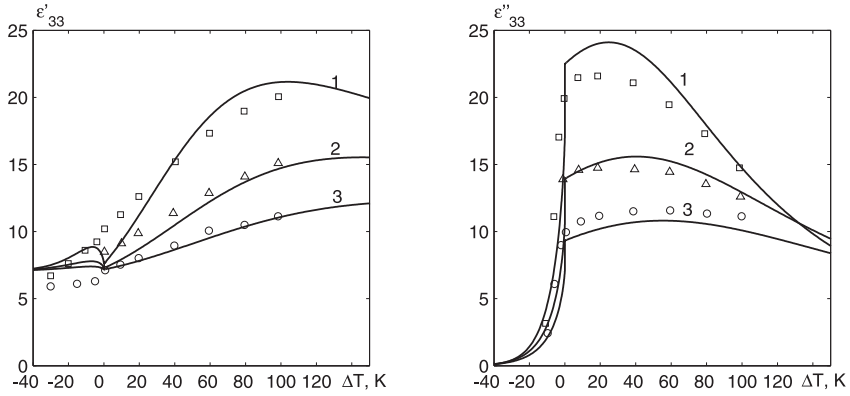

Figure 7. The temperature dependence of ε'_{33} and ε''_{33} in $K(H_{0.36}D_{0.64})_2PO_4$ at different frequencies ν (GHz) [35]: 154.2 – 1, □; 249.0 – 2, △; 372.0 – 3, ○. Symbols are experimental points; lines are the theoretical values.

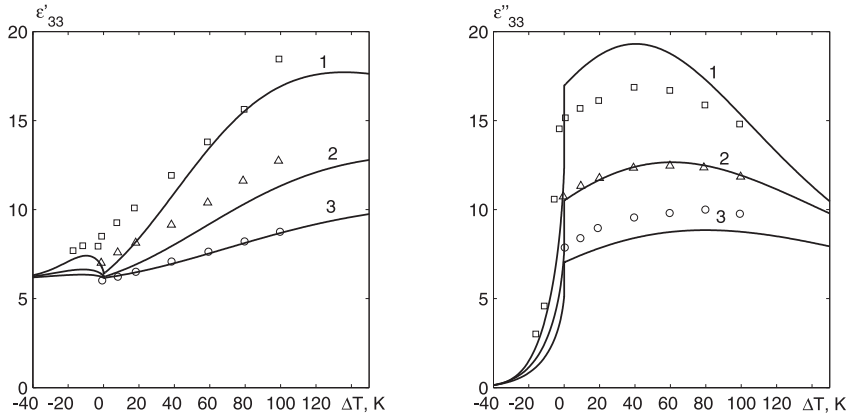

Figure 8. The temperature dependence of ε'_{33} and ε''_{33} in $K(H_{0.16}D_{0.84})_2PO_4$ at different frequencies ν (GHz) [35]: 154.2 – 1, □; 249.0 – 2, △; 372.0 – 3, ○. Symbols are experimental points; lines are the theoretical values.

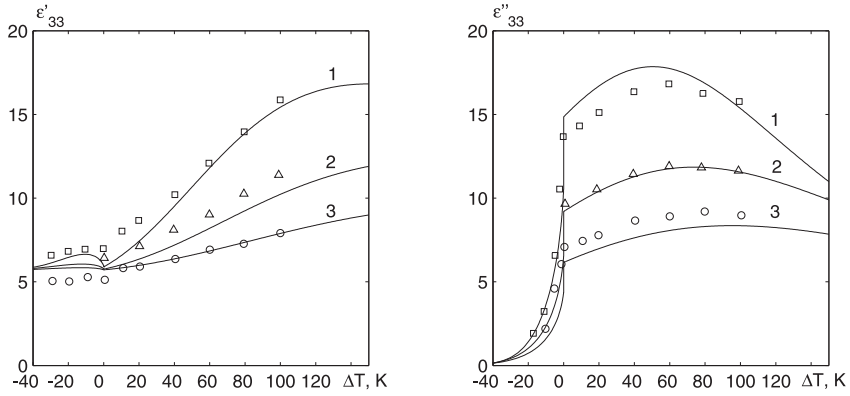

Figure 9. The temperature dependence of ε'_{33} and ε''_{33} in $K(H_{0.07}D_{0.93})_2PO_4$ at different frequencies ν (GHz) [35]: 154.2 – 1, □; 249.0 – 2, △; 372.0 – 3, ○. Symbols are experimental points; lines are the theoretical values.

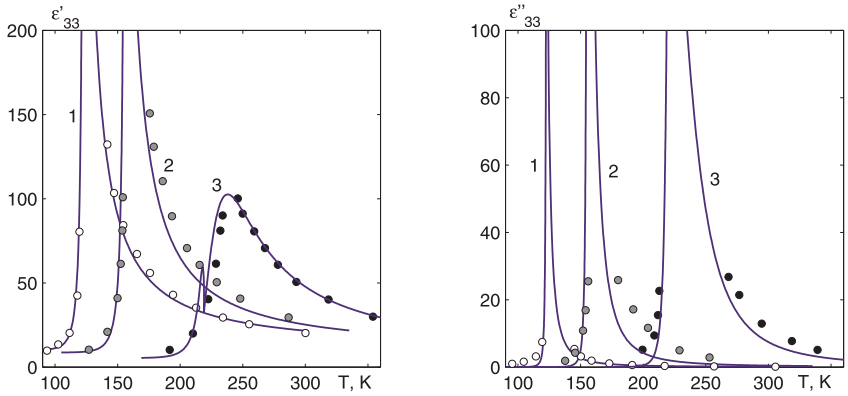

Figure 10. The temperature dependence of ε'_{33} and ε''_{33} in $K(H_{1-x}D_x)_2PO_4$ at ν=9.2 GHz and for different x [36]: 0.0 – 1, ○; 0.29 – 2, ●; 0.99 – 3, ●. Symbols are experimental points; lines are the theoretical values.

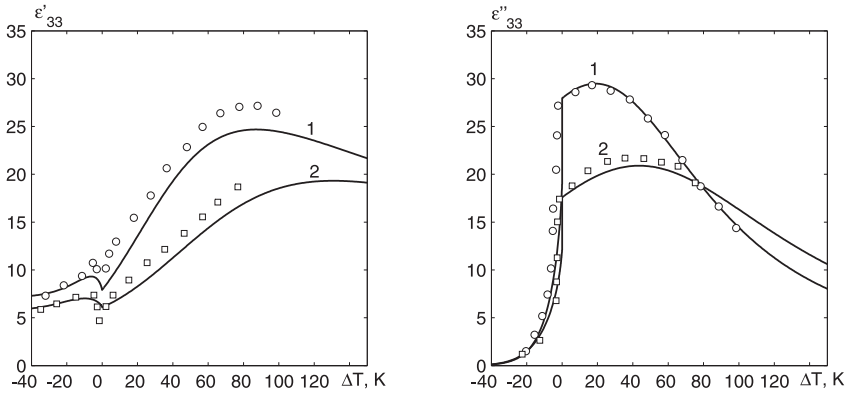

Figure 11. The temperature dependence of ε'_{33} and ε''_{33} in $K(H_{1-x}D_x)_2PO_4$ at ν=138.6 GHz and for different x [43]: 0.63 – 1, ○; 0.91 – 2, □. Symbols are experimental points; lines are the theoretical values.

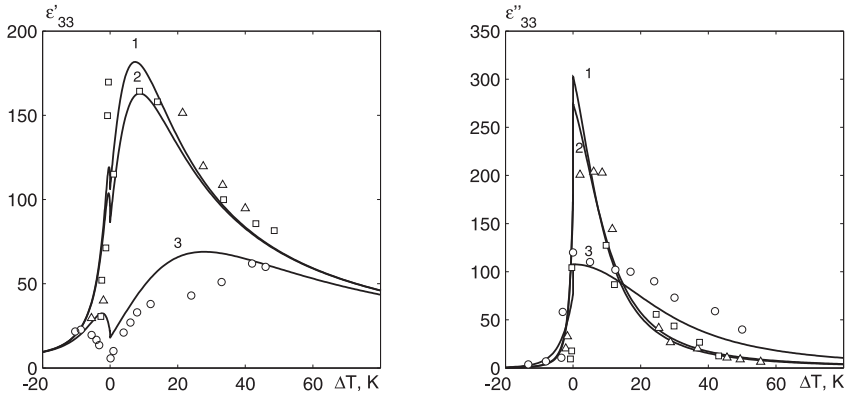

Figure 12. The temperature dependence of ε'_{33} and ε''_{33} in $K(H_{0.22}D_{0.78})_2PO_4$ at different frequencies ν (GHz) [38]: 8.6 – 1, △; 9.7 – 2, □; 26.5 – 3, ○. Symbols are experimental points; lines are the theoretical values.

data of [37], this is the low-frequency tail. Further experimental measurements of $\varepsilon^*_{33}(\nu, T)$ at $\nu > 10$ are required to evaluate the validity of the calculated $\varepsilon^*_{33}(\nu, T)$.

The most graphic illustration of the dispersion of the real and imaginary parts of the dielectric permit-

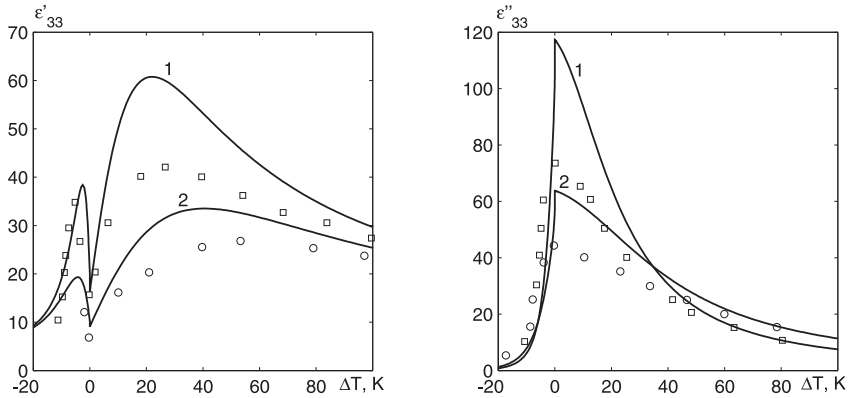

Figure 13. The temperature dependence of ε'_{33} and ε''_{33} in RbH_2PO_4 at different frequencies ν (GHz) [42]: 198.0 – 1, □; 366.0 – 2, ○. Symbols are experimental points; lines are the theoretical values.

tivity $\varepsilon^*_{33}(\omega, T)$ in $M(H_{1-x}D_x)_2XO_4$ would be their frequency-temperature plots drawn in wide frequency and temperature ranges. Such plots for theoretical dependencies along with the experimental points are presented in figures 14, 15 for $K(H_{0.07}D_{0.93})_2PO_4$, in figures 16, 17 for RbH_2PO_4, and in figures 18, 19 for KH_2AsO_4.

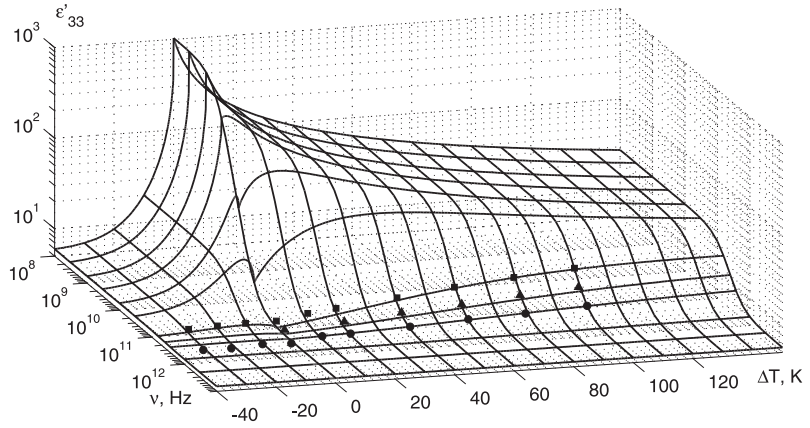

Figure 14. The frequency-temperature dependence of ε'_{33} in $K(H_{0.07}D_{0.93})_2PO_4$. ■, ▲, ● – [35]. Symbols are experimental points; lines are the theoretical values.

Let us analyse the changes in the real and imaginary parts of $\varepsilon^*_{33}(\omega)$ in the $M(H_{1-x}D_x)_2XO_4$ crystals at replacing H → D, K → Rb, and P → As. At $\Delta T = +0$ K, the dispersion frequency [i.e., the frequency of the maximum of $\varepsilon''_{33}(\omega)$] is 33.2 in KH_2PO_4, 1.93 in KD_2PO_4, 20.5 in RbH_2PO_4, and 20.8 in KH_2AsO_4. The linewidth [i.e., the difference between frequencies of the maximum and half maximum of $\varepsilon''_{33}(\omega)$] is 12.0 GHz in KH_2PO_4, 4.8 in KD_2PO_4, 7.8 in RbH_2PO_4, and 7.2 in KH_2AsO_4.

The temperature dependencies of the inverse relaxation time $(\tau^z_1)^{-1}$ in $K(H_{1-x}D_x)_2PO_4$ along with the values estimated from different experimental measurements are presented in figure 20. The calculated values of the relaxation times $\tau^z_{2,3,4}$, in contrast to τ^z_1, are unlikely to depend on temperature and are much smaller than the value of τ^z_1. The theory provides a satisfactory agreement with the experiment for temperature curves of the relaxation time. A certain difference between the relaxation times estimated from the dielectric permittivity and ultrasound measurements is due to the contributions into attenuation from the mechanisms irrelevant for the permittivity (e.g., scattering by admixtures).

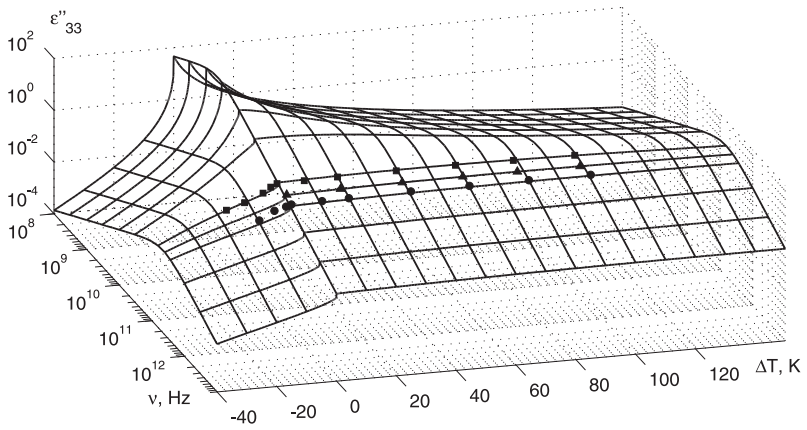

Figure 15. The frequency-temperature dependence of ε''_{33} in $K(H_{0.07}D_{0.93})_2PO_4$. ■, ▲, ● – [35]. Symbols are experimental points; lines are the theoretical values.

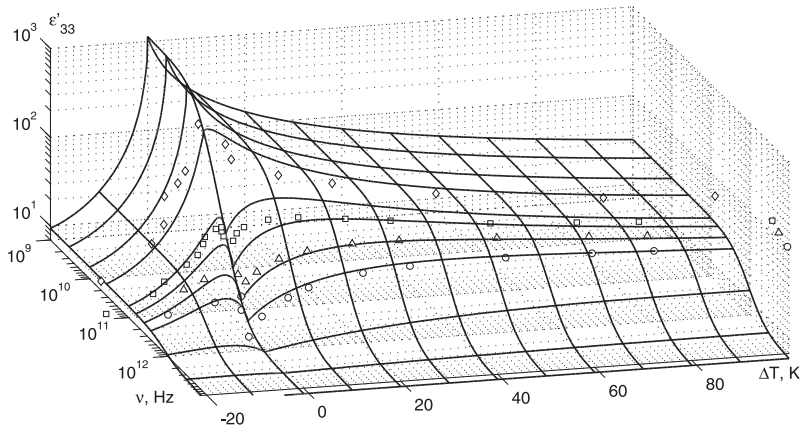

Figure 16. The frequency-temperature dependence of ε'_{33} in RbH_2PO_4. ◇ – [40]; □, △, ○ – [41]. Symbols are experimental points; lines are the theoretical values.

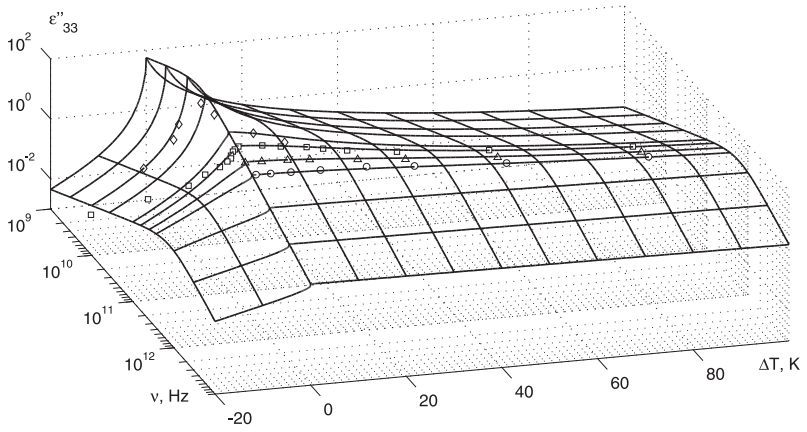

Figure 17. The frequency-temperature dependence of ε''_{33} in RbH_2PO_4. ◇ – [40]; □, △, ○ – [41]. Symbols are experimental points; lines are the theoretical values.

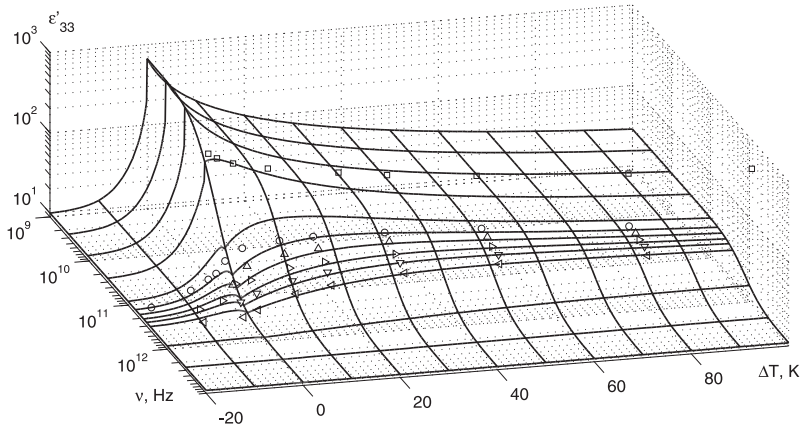

Figure 18. The frequency-temperature dependence of ε'_{33} in KH_2AsO_4. □ – [36]; ○, △, ▷, ▽, ◁ – [41]. Symbols are experimental points; lines are the theoretical values.

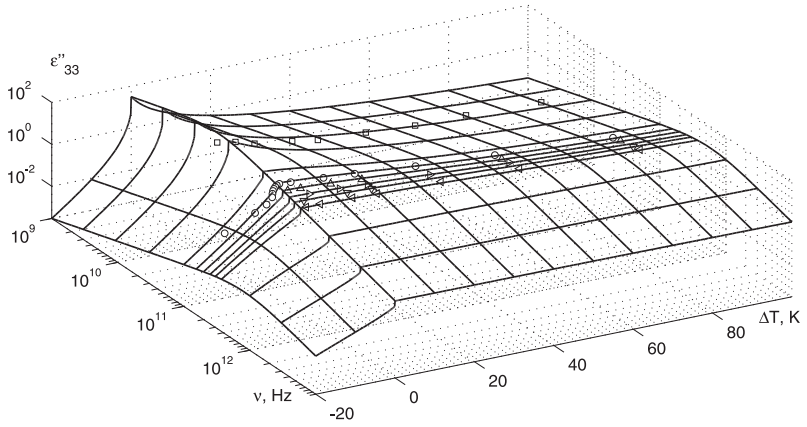

Figure 19. The frequency-temperature dependence of ε''_{33} in KH_2AsO_4. □ – [36]; ○, △, ▷, ▽, ◁ – [41]. Symbols are experimental points; lines are the theoretical values.

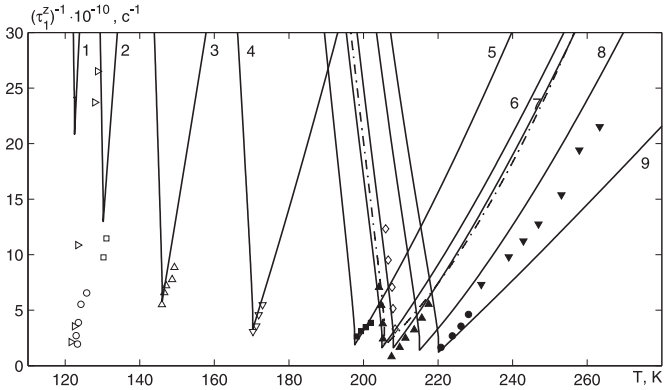

Figure 20. The temperature dependence of the inverse polarization relaxation time at different x: 0.0 – 1, ▷ [47], ◁ [48], ○ [49]; 0.07 – 2, □ [50]; 0.21 – 3, △ [50]; 0.43 – 4, ▽ [50]; 0.72 – 5, ■ [50]; 0.805 – 6, ▲ [51]; 0.84 – 7, ◇ [52]; 0.93 – 8, ▼ [48]; 1.0 – 9, ● [53]. Symbols are experimental points; lines are the theoretical values.

5. Conclusions

Within the framework of the modified proton ordering model, taking into account a linear over the strain ε_6 contribution into the energy of the proton subsystem, and using the four-particle cluster approximation, we calculate the longitudinal dynamic characteristics of mechanically clamped crystals of the KH_2PO_4 family. For the partially deuterated crystals $M(H_{1-x}D_x)_2XO_4$, these characteristics are obtained within the mean crystal approximation. The data for $\varepsilon'_{33}(\nu, T)$ and $\varepsilon''_{33}(\nu, T)$ presented by different groups of experimentalists are analyzed and systematized. At the proper choice of the theory parameters for the $M(H_{1-x}D_x)_2XO_4$ crystals, we obtain a good quantitative description of the available experimental data for $\varepsilon'_{33}(\nu, T)$ and $\varepsilon''_{33}(\nu, T)$. For the first time, the dispersion of the longitudinal dynamic dielectric permittivity of clamped crystals of the KH_2PO_4 family is explored in wide temperature and frequency ranges. It should be noted that the effect of piezoelectric coupling on the dielectric characteristics of these crystals is essential. In the present paper, the observed temperature behavior of $\varepsilon'_{33}(\nu, T)$ in the phase transition region at different frequencies has been appropriately described for the first time.

References

1. Levitsky R.R., Zachek I.R., Volkov. A.A., Kozlov G.V., Lebedev S.P. Preprint of the Bogolyubov Institute for Theoretical Physics, ITP–80–13R, Kyiv, 1980 (in Russian).
2. Yoshimitsu K., Matsubara T., Suppl. Progr. Theor. Phys., 1968, **E68**, 109; doi:10.1143/PTPS.E68.109.
3. Poplavko Y.M., Physics of Dielectrics. Vyshcha Shkola, Kyiv, 1980 (in Russian).
4. Vaks V.G., Introduction into Microscopic Theory of Ferroelectrics. Moskow, 1973 (in Russian).
5. Blinc R., Zeks B., Ferroelectrics and Antiferroelectrics. Lattice dynamics. Moskow, 1975 (in Russian).
6. Glauber J., J. Math. Phys., 1963, **4**, No. 2, 294; doi:10.1063/1.1703954.
7. Levitsky R.R., Zachek I.R., Varanitsky V.I. Preprint of the Bogolyubov Institute for Theoretical Physics, ITP–79–11E, Kiev, 1979.
8. Zachek I.R., Levitsky R.R., Teor. Mat. Fiz., 1980, **43**, No. 1, 128 (in Russian) [Theor. Math. Phys., **43**, No. 1, 364; doi:10.1007/BF01018473].
9. Levitsky R.R., Zachek I.R., Varanitsky V.I., Ukr. J. Phys., 1980, **25**, No. 12, 1961 (in Russian).
10. Levitsky R.R., Zachek I.R., Mits Ye.V. Preprint of the Bogolyubov Institute for Theoretical Physics, ITP–87–114R, Kyiv, 1987 (in Russian).
11. Zachek I.R., Mits Ye.V., Levitsky R.R. Preprint of the Bogolyubov Institute for Theoretical Physics, ITP–89–7R, Kyiv, 1987 (in Russian).
12. Levitskii R.R., Zachek I.R., Vdovych A.S., Sorokov S.I., Condens. Matter Phys., 2009, **12**, No. 1, 75; doi:10.5488/CMP.12.1.75.
13. Stasyuk I.V., Levitskii R.R., Korinevskii N.A., Phys. Status Solidi B, 1979, **91**, No. 2, 541; doi:10.1002/pssb.2220910219.
14. Levitsky R.R., Stasyuk I.V., Korinevsky H.A., Ferroelectrics, 1978, **21**, 481; doi:10.1080/00150197808237303.
15. Korinevskii N.A., Levitskii R.R., Teor. Mat. Fiz., 1980, **42**, No. 3, 416 (in Russian) [Theor. Math. Phys., 1980, **42**, No. 3, 274; doi:10.1007/BF01018631].
16. Yukhnovskii I.R., Levitskii R.R., Sorokov S.I., Derzhko O.V., Izv. AN SSSR, ser. fiz., 1991, **55**, No. 3, 481 (in Russian).
17. Levitskii R.R., Sorokov S.I., Baran O.R., Condens. Matter Phys., 2000, **3**, No. 3, 515.
18. Levitskii R.R., Sorokov S.I. Preprint of the Bogolyubov Institute for Theoretical Physics, ITP–88–34R, Kyiv, 1988 (in Russian).
19. Levitskii R.R., Sorokov S.I., Moina A.P. Preprint of the Institute for Condensed Matter Physics, ICMP–97–24U, Lviv, 1997 (in Ukrainian).
20. Yomosa Sh., Nagamiya T., Progr. Theor. Phys., 1949, **4**, No. 3, 263; doi:10.1143/PTP.4.263.
21. Slater J.C., J. Chem. Phys., 1941, **9**, No. 1, 16; doi:10.1063/1.1750821.
22. Stasyuk I.V., Biletskii I.N. Preprint of the Bogolyubov Institute for Theoretical Physics, ITP–83–93R, Kyiv, 1983 (in Russian).
23. Stasyuk I.V., Biletskii I.N., Styagar O.N., Ukr. J. Phys., 1986, **31**, No. 4, 567.
24. Stasyuk I.V., Levitskii R.R., Zachek I.R., Moina A.P., Phys. Rev. B, 2000, **62**, No. 10, 6198; doi:10.1103/PhysRevB.62.6198.
25. Levitskii R.R., Lisnii B.M., J. Phys. Stud., 2003, **7**, No. 4, 431 (in Ukrainian).
26. Levitsky R.R., Zachek I.R., Vdovych A.S., Moina A.P., J. Phys. Stud., 2010, **14**, No. 1, 1701.
27. Levitskii R.R., Lisnii B.M., Phys. Status Solidi B, 2004, **241**, No. 6, 1350.

28. Stasyuk I.V., Levitskii R.R., Moina A.P., Lisnii B.M., Ferroelectrics, 2001, **254**, 213; doi:10.1080/00150190108215002.
29. Lisnii B.M., Levitskii R.R., Baran O.R., Phase Transitions, 2007, **80**, 25; doi:10.1080/01411590701315591.
30. Stasyuk I.V., Levitskii R.R., Moina A.P., Velychko O.V., Ukr. J. Phys., 2008, **4**, 3 (in Ukrainian).
31. Levitskii R.R., Lisnii B.M., J. Phys. Stud., 2002, **6**, No. 1, 91 (in Ukrainian).
32. Levitsky R.R., Zachek I.R., Moina A.P., Vdovych A.S., Condens. Matter Phys., 2008, **11**, No. 3, 555.
33. Stasyuk I.V., Levitskii R.R., Zachek I.R., Vdovych A.S., The SSS Physical Proceeding, 2011, **8**, 533.
34. Levitskii R.R., Zachek I.R., Vdovych A.S. Preprint of the Institute for Condensed Matter Physics, ICMP–06–08U, Lviv, 2006 (in Ukrainian).
35. Volkov A.A., Kozlov G.V., Lebedev S.P., Velychko I.A., Fiz. Tverd. Tela, 1979, **21**, No. 11, 3304 (in Russian).
36. Kaminow I.P., Phys. Rev., 1965, **138**, A1539; doi:10.1103/PhysRev.138.A1539.
37. Hill R.M., Ichiki S.K., Phys. Rev., 1963, **132**, No. 4, 1603; doi:10.1103/PhysRev.132.1603.
38. Pereverzeva L.P., Poplavko Yu.M., Rez I.S., Kuznetsova L.I., Kristallografiya, 1976, **21**, No. 5, 981 (in Russian).
39. Blinc R., Schmidt V.H., Ferroelectr. Lett. Sect., 1984, **1**, 119; doi:10.1080/07315178408202409.
40. Pereverzeva L.P., Izv. AN SSSR, ser. fiz., 1971, **35**, No. 12, 2613 (in Russian).
41. Volkov A.A., Kozlov G.V., Lebedev S.P., Prokhorov A.M., Ferroelectrics, 1980, **25**, No. 1–4, 531; doi:10.1080/00150198008207063.
42. Meriakri V.V., Ushatkin E.F. Investigation of inorganic materials by submillimeter spectroscopy metods. – In: Physical methods of investigation of inorganic materials. Moscow, Nauka, 1981, p. 195–205 (in Russian).
43. Gauss K.E., Happ H., Phys. Status Solidi B, 1976, **78**, No. 1, 133; doi:10.1002/pssb.2220780111.
44. Skalyo J., Frazer B.C. Jr., Shirane G., Daniels W.B., J. Phys. Chem. Solids, 1969, **30**, No. 8, 2045; doi:10.1016/0022-3697(69)90183-8.
45. Gauss K.E., Happ H., Rother G., Phys. Status Solidi B, 1975, **72**, No. 2, 623; doi:10.1002/pssb.2220720220.
46. Meriakri V.V., Poplavko Yu.M., Ushatkin E.F., Zh. Tekh. Fiz., 1974, **44**, No. 5, 1111 (in Russian).
47. Garland C.W., Novotny D.B., Phys. Rev., 1969, **177**, No. 2, 971; doi:10.1103/PhysRev.177.971.
48. Vajda D., Acta Phys. Slov., 1980, **30**, No. 1, 99.
49. Litov E., Garland C.M., Phys. Rev. B, 1970, **2**, No. 11, 4597; doi:10.1103/PhysRevB.2.4597.
50. Kasahara M., Tatsuzaki I., J. Phys. Soc. Jpn., 1981, **50**, No. 2, 551; doi:10.1143/JPSJ.50.551.
51. Litov E., Uehling E.A., Phys. Rev. B, 1970, **1**, No. 9, 3713; doi:10.1103/PhysRevB.1.3713.
52. Shimshoni M., Harnik E., Phys. Lett. A, 1970, **32**, No. 5, 321; doi:10.1016/0375-9601(70)90526-8.
53. Reese R.L., Fritz J.J., Cummins H.Z., Phys. Rev. B, 1973, **7**, No. 9, 4165; doi:10.1103/PhysRevB.7.4165.

Поздовжня релаксація механічно затиснутих кристалів типу KH_2PO_4

Р.Р. Левицький[1], І.Р. Зачек[2], А.С. Вдович[1]

[1] Інститут фізики конденсованих систем НАН України вул. Свєнціцького, 1, Львів, 79011, Україна,

[2] Національний університет "Львівська політехніка" вул. С. Бандери 12, 79013, Львів, Україна

У рамках модифікованої моделі протонного впорядкування сеґнетоактивних кристалів сім'ї KH_2PO_4 з врахуванням лінійного за деформацією внеску ε_6 в енергію протонної системи в наближенні чотиричастинкового кластера в межах динамічної моделі Глаубера отримано вираз для поздовжньої динамічної діелектричної проникності механічно затиснутого кристалу. При належному виборі параметрів теорії отримано добрий кількісний опис наявних експериментальних даних для цих кристалів.

Ключові слова: *сегнетоелектрики, кластерне наближення, діелектрична проникність, часи релаксації*